Spectroscopic and laser gain properties of the Nd^{3+}:β'-$Gd_2(MoO_4)_3$ non-linear crystal

2000 J. Phys.: Condens. Matter 12 9699

(http://iopscience.iop.org/0953-8984/12/46/316)

J. Phys.: Condens. Matter **12** (2000) 9699–9714. Printed in the UK PII: S0953-8984(00)15684-X

Spectroscopic and laser gain properties of the Nd^{3+}:β'-$Gd_2(MoO_4)_3$ non-linear crystal

D Jaque†, J Findensein‡, E Montoya§, J Capmany‖, A A Kaminskii¶, H J Eichler‡ and J García Solé§

† Departamento de Física de Materiales, Universidad Complutense de Madrid, Ciudad Universitaria, 28040, Madrid, Spain

‡ Optisches Institut, Technische Universität Berlin, Strasse des 17 Juni 135, D-10623 Berlin, Germany

§ Departamento de Física de Materiales, Universidad Autónoma de Madrid, Cantoblanco, 28049 Madrid, Spain

‖ Departamento de Física y Arquitectura de Computadores, Universidad Miguel Hernandez 3022, Elche, Spain

¶ Institute of Crystallography, Russian Academy of Sciences, Leninsky Prospekt 59, 117333 Moscow, Russia

Received 20 July 2000, in final form 10 October 2000

Abstract. In this paper the polarized optical spectra (absorption and fluorescence) of the Nd^{3+} ion in the $Gd_2(MoO_4)_3$ non-linear crystal have been investigated at low (10 K) and room temperature. Results obtained from low-temperature experiments have been used to obtain the energy level diagram and also to identify two non-equivalent centres of Nd^{3+} ions in this crystal. The Judd–Ofelt formalism is applied to the room temperature absorption spectra, and the relevant spectroscopic parameters (quantum efficiency and emission cross section) for laser applications have been estimated. Infrared-to-visible up-conversion in this host crystal is reported for the first time. Finally, continuous-wave laser experiments are carried out and from them, optimal conditions for generation of green laser light are established.

1. Introduction

The increasing interest in small and compact diode-pumped lasers in the visible spectral domain has encouraged research on new solid-state laser systems based on non-linear crystals (second- or third-order non-linearity) [1–3]. These crystals, when activated with trivalent rare-earth ions, provide the possibility of realizing diode-pumped visible lasers by means of self-frequency doubling (SFD) or by stimulated Raman scattering (SRS), both non-linear processes based on the main infrared laser radiation lines.

Acentric $Gd_2(MoO_4)_3$ crystals [4] are well known as ferroelectric and ferroelastic materials. Crystals with these two properties have several potential applications in opto-electronics. Examples include use in page composers, memory cells, and low-speed mechanical positioning systems. When combined with Nd^{3+} ions, these crystals provide an excellent gain medium for laser oscillation in the infrared (1 and 1.3 μm) produced by pumping with a laser diode, leading to compact laser devices [5–8]. In addition, they are non-linear crystals with considerable quadratic ($\chi^{(2)}$) and cubic ($\chi^{(3)}$) non-linear optical susceptibilities. Second-harmonic generation (SHG) has been demonstrated, showing a wide tunability range (from 470 up to 800 nm), by using a pulsed laser source [9]. Continuous-wave SFD laser action

0953-8984/00/469699+16$30.00

in the green from a Nd:$Gd_2(MoO_4)_3$ crystal has been demonstrated by using different excitation schemes [8, 10]. The high cubic ($\chi^{(3)}$) non-linear susceptibility provides the possibility of realizing crystalline laser Raman shifters [11]. In fact, up to five Stokes and five anti-Stokes lines have been obtained in picosecond SRS experiments with a total conversion efficiency of about 70% [12]. Interactions of SHG and SRS, as well as a new effect, which has been called 'quasi-hyper-SRS', have been previously observed in this crystal [12].

Most of the work performed on neodymium-doped gadolinium molybdate is focused on the potential integration of this crystal in optical devices. Only a few works have partially dealt with the optical properties of incorporated Nd^{3+} ions [13]. Thus, a detailed characterization of the spectroscopy of this material is still lacking. This characterization is necessary for a full understanding of the laser gain properties of this ion–host combination. Indeed, the information obtained from spectroscopic experiments can be used to determine the conditions needed for optimum device efficiency.

This paper presents a systematic investigation of the optical (absorption and luminescence) bands of Nd^{3+} in $Gd_2(MoO_4)_3$. As a result of careful investigation of the location of these bands, a table of the energy levels of the Nd^{3+} ion, conveniently labelled, is produced. In addition, low-temperature absorption spectra are used to demonstrate the existence of two non-equivalent Nd^{3+} centres. Polarized emission spectra for the metastable state $^4F_{3/2}$ are used to estimate the ratio of integrated intensities and, from them, the spectroscopic quality parameter (χ). Analysis of the band intensities and fluorescence lifetime is used to estimate some relevant laser parameters of the main laser channels. Infrared-to-visible up-converted fluorescence is reported and the mechanisms responsible for this luminescence are discussed. Finally, continuous-wave (CW) laser gain experiments have been carried out in order to determine the optimum experimental conditions for visible laser light generation.

2. Crystal properties and experimental details

$Gd_2(MoO_4)_3$ crystals doped with Nd^{3+} were grown by the Czochralski technique at the Russian Institute of Crystallography (Moscow). The neodymium concentration was determined by means of total-reflection x-ray fluorescence (TRXF) to be 3.44 at.%, which corresponds to 1.2×10^{20} ions cm^{-3}. Below the Curie temperature ($T_c = 159$ °C) $Gd_2(MoO_4)_3$ has an orthorhombic structure (space group C^8_{2v}–$Pba2$, ferroelectric β'-phase) and above T_c the unit cell becomes tetragonal (D^3_{2d}–$P42_1m$, paraelectric β-phase). In this work we are dealing exclusively with crystals in the β'-phase. X-ray diffraction experiments were carried out and the results show a single orthorhombic phase with no evidence of inclusions of the tetragonal phase. The crystal lattice parameters of this β'-phase at 20 °C (in Å) are: $a = 10.39$, $b = 10.41$ and $c = 10.67$. Since $a \simeq b \neq c$, this crystal can be considered as a quasi-uniaxial crystal with a positive birefringence ($n_o < n_e$) at any temperature [9, 12]. In fact, polarized absorption spectra have shown that the a- and b-directions are equivalent.

Plate samples of Nd:$Gd_2(MoO_4)_3$ were cut from the crystal boule with the c-axis contained in one of its faces, in such a way that σ ($\boldsymbol{E} \perp \boldsymbol{c}$) and π ($\boldsymbol{E} \parallel \boldsymbol{c}$) spectra could be measured. For laser gain experiments a 4.5 mm long crystal cut along the phase-matching direction for self-frequency doubling the fundamental laser line at 1060 nm ($\theta \approx 60°$) [9, 12] was used. Crystal faces were carefully polished up to laser quality. No antireflection coatings were deposited on them.

The polarized optical absorption spectra were measured with an Hitachi spectrophotometer (model U-3501) using a calcite polarizer.

For the CW fluorescence (excitation and emission) spectra and laser gain experiments, a Ti:sapphire (Spectra Physics, model 3900) tunable laser was used, while experiments under

pulsed excitation were performed by using a high-power (20 mJ, 10 ns pulse width) optical parametric oscillator (MOPO, Spectra Physics model 730). The luminescence was dispersed by a 500M SPEX monochromator (spectral resolution $\simeq 0.05$ nm) and detected with a cooled photomultiplier or a calibrated Ge detector (depending upon the spectral range). The signals were recorded by using an EG&G lock-in amplifier. The decay time measurements were performed using the averaging facilities of a Tektronix 2400 digital storage oscilloscope. For these experiments, the monochromator slits were totally opened, so the spectral resolution was around 2 nm. Low-temperature spectra (10 K) were taken by mounting the samples in a Leybold temperature-controlled closed-He-cycle cryostat.

For laser gain experiments a hemispherical cavity was used. A plane input mirror (high reflectance at 1.06 μm) and 10 cm radius-of-curvature output mirrors (99.7, 99, 98 and 96% reflectance at 1.06 μm) were used. The pump beam from the Ti:sapphire laser was focused onto the sample by a 5 cm focal lens. The spectral shape of the infrared laser beam was analysed in real time by means of an Optical Multichannel Analyser (Otsuka MCPD 1100).

3. Results and discussion

3.1. Spectroscopic measurements

3.1.1. Low-temperature spectra. As for other host crystals [3, 13], the absorption and luminescence spectra of Nd^{3+} in $Gd_2(MoO_4)_3$ consist of transitions among the Stark sublevels of $^{2S+1}L_J$ states within the $4f^3$ configuration of the ion.

Because the Nd^{3+} ions replace Gd^{3+} lattice cations, the Nd^{3+} ions incorporated are expected to retain the environment of the occupied lattice site. Within this local symmetry all $^{2S+1}L_J$ states are split by the crystal field into the maximum number of Kramers levels $(2J+1)/2$ [14].

Figure 1(a) shows the 10 K unpolarized absorption coefficient spectrum of the crystal Nd:$Gd_2(MoO_4)_3$ over the energy range from 1.1×10^4 to 3×10^4 cm^{-1}. The bands shown in figure 1(a) correspond to transitions from the ground state (the lower Stark level of the $^4I_{9/2}$ manifold) to upper states. The excited states involved in the different sets of transitions have been indicated. For Stark components above 30 000 cm^{-1} the absorption edge becomes dominant and no more states can be accessed. In order to detect the energy levels of the $^4I_{9/2,11/2,13/2}$ states, unpolarized emission spectra at 10 K were recorded. Figure 1(b) shows the unpolarized emission spectra at 10 K when the crystal is excited at 800 nm by using the Ti:sapphire laser. Nd^{3+} ions are excited from the ground to the $^4F_{5/2}$ state. Then, a fast non-radiative decay occurs in such a way that the $^4F_{3/2}$ metastable state is populated. This allowed us to determine the energy levels of the $^4I_{9/2,11/2,13/2}$ states.

Let us focus our attention on the absorption band corresponding to transitions from the ground state to the $^2P_{1/2}$ excited state. As was mentioned before, the local symmetry makes the $^{2S+1}L_J$ state split into the maximum number of Kramers levels $(2J+1)/2$. Thus, for $^2P_{1/2}$ the maximum number of Kramers levels is one (it is not split by the crystalline field). Figure 2(a) shows the low-temperature absorption spectra corresponding to the $^2P_{1/2}$ excited state. Two sharp transitions can easily be observed. In principle, this fact can be explained in terms of two non-equivalent centres of Nd^{3+} ions in the crystal lattice. Different Nd^{3+} locations in the lattice cause different crystal fields. As a consequence, the energy of the Stark levels can be modified from one lattice site to another. The existence of two non-equivalent Nd^{3+} centres can also be appreciated in the $^4I_{9/2} \rightarrow {}^4F_{3/2}$ absorption spectra (see figure 2(b)). In this case the maximum number of Kramers levels is two, but up to four different transitions are observed.

All of the energy levels have been tabulated in table 1. As can be appreciated, 123 energy levels have been detected, although no more than 87 were expected. The presence of

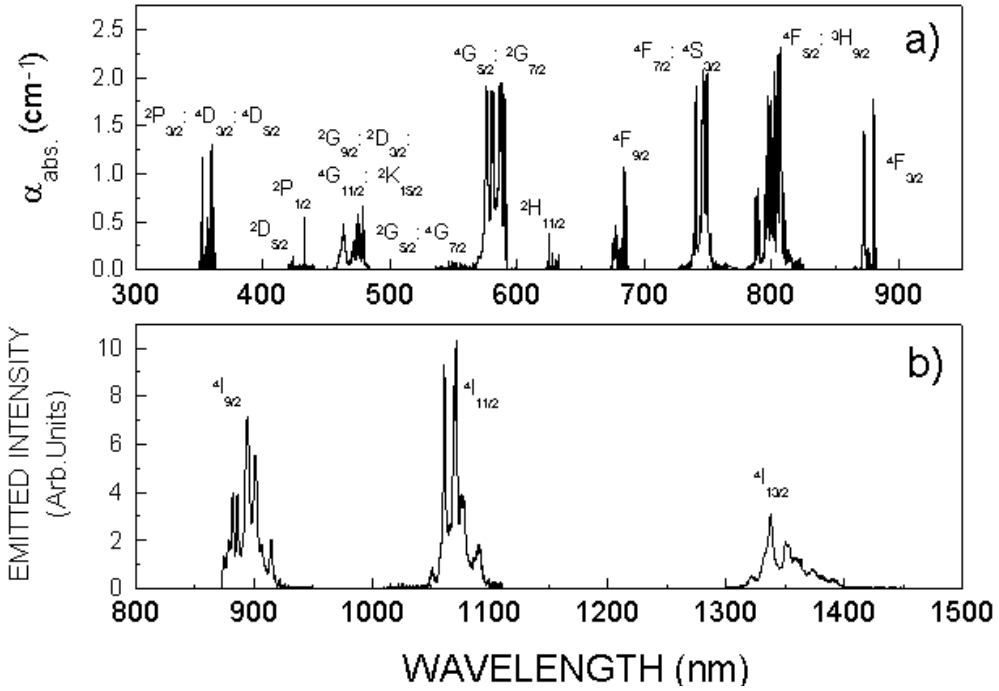

Figure 1. Low-temperature (10 K) unpolarized absorption (a) and emission (b) spectra for Nd^{3+} ions in $Gd_2(MoO_4)_3$. The transitions associated with each band are indicated.

two non-equivalent centres increases the number of Nd energy states in the Nd:$Gd_2(MoO_4)_3$ system.

The $^4F_{3/2}$ fluorescence lifetime, τ_F, has been measured in the 15–300 K temperature range. Even for low-temperature measurements, the lifetime obtained was independent of both the excitation and emission wavelengths. The fluorescence lifetime has been found to be independent of temperature with an averaged value of 165 ± 10 μs (see the inset in figure 3). Figure 3 shows the time evolution of the $^4F_{3/2}$ fluorescence at room (300 K) temperature. Due to band thermal broadening, both Nd centres are contributing to the fluorescence signal; nevertheless, the time evolution can be nicely fitted to a single exponential decay indicating that the $^4F_{3/2}$ total transition probabilities ($1/\tau_F$) are roughly the same for the two centres.

3.1.2. Room temperature absorption spectra. Judd–Ofelt intensity parameters. The polarized (σ and π) absorption spectra have also been recorded at room temperature in order to estimate the Judd–Ofelt (JO) intensity parameters, thus providing a first estimate of the radiative rates [15, 16]. Figure 4 shows the room temperature σ and π absorption spectra in the wavelength range from 1100 to 280 nm. As for the low-temperature case, no absorptions are observed for wavelengths shorter than 300 nm due to the onset of the absorption edge. The room temperature condition leads to thermal broadening of the absorption lines as well as the appearance of hot side bands originating from thermal population of excited levels within the ground state $^4I_{9/2}$. This is, anyway, necessary in order to fulfil the JO assumption of equal population for all of the levels of the same state [15, 16].

From data displayed in figure 4, the absorption line strengths of the ED (electrical dipole) transitions departing from the ground state can be measured. The JO formalism for anisotropic

Table 1. Energy levels of the Nd^{3+} ions in Nd^{3+}:$Gd_2(MoO_4)_3$ crystal.

State	Energy (cm^{-1})	State	Energy (cm^{-1})	State	Energy (cm^{-1})
$^4I_{9/2}$	0	$^4F_{7/2}$:$^4S_{3/2}$	13291	$^2G_{5/2}$:$^4G_{7/2}$	17760
	53		13339		17781
	98		13351		17862
	148		13389		17894
	250		13406		17960
	337		13445		18002
	399		13456		18128
	503		13493		18184
			13497		18211
$^4I_{11/2}$	1839		13506		18305
	1934		13535		18314
	2005				
	2022	$^4F_{9/2}$	14589	$^2G_{9/2}$:$^2D_{3/2}$:$^4G_{11/2}$:$^2K_{15/2}$	20857
	2059		14595		20878
	2078		14626		20889
	2180		14639		20927
	2195		14693		20938
			14701		21032
$^4I_{13/2}$	3787		14756		21060
	3856		14769		21103
	3884		14801		21191
	3950				21208
	3968	$^2H_{11/2}$	15814		21243
	4006		15818		21277
	4023		15832		21369
	4073		15840		21484
	4118		15859		21527
	4165		15936		21557
			15990		21592
			16005		21666
$^4F_{3/2}$	11358				21702
	11367	$^4G_{5/2}$:$^2G_{7/2}$	16903		
	11408		16923	$^2P_{1/2}$	23081
	11458		16951		23132
			16967		
$^4F_{5/2}$:$^3H_{9/2}$	12303		16975	$^2D_{5/2}$	23599
	12340		17016		23609
	12386		17056		23617
	12399		17099		23682
	12431		17150		23688
	12465		17206		
	12474		17242	$^2P_{3/2}$:$^4D_{3/2}$:$^4D_{5/2}$	27666
	12498		17253		27710
	12514		17325		27731
	12542		17370		27803
	12572				27834
	12663				27895
	12698				27925
					28091
					28214
					28396
					28418
					28446

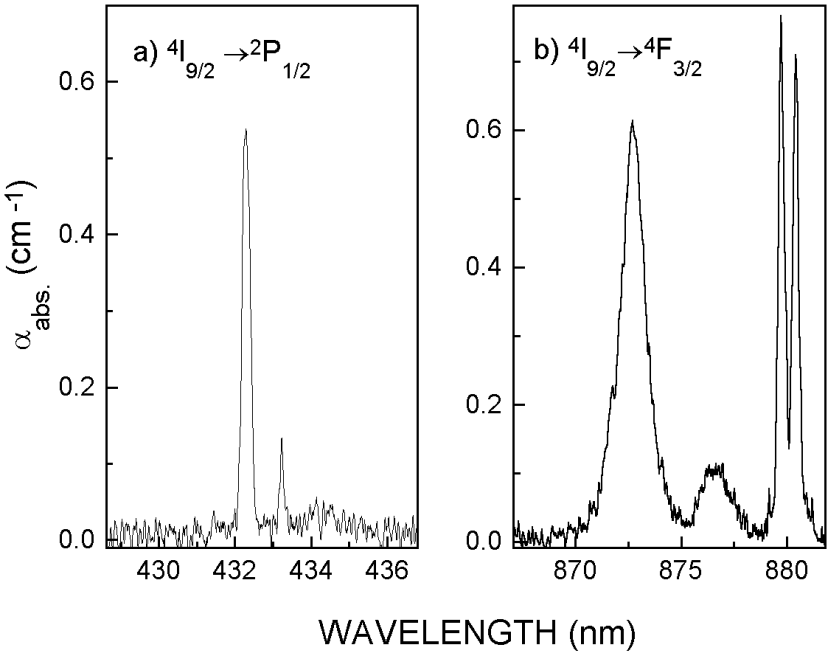

Figure 2. Detailed low-temperature absorption spectra corresponding to the $^4I_{9/2} \rightarrow {}^2P_{1/2}$ (a) and $^4I_{9/2} \rightarrow {}^4F_{3/2}$ (b) transitions.

crystals can then be applied. This will allow us to obtain a first estimate of the radiative transition probabilities and branching ratios for any two states of the Nd:$Gd_2(MoO_4)_3$ system.

For uniaxial crystals (as considered here) the absorption strength $S(J \rightarrow J')$ going from the ground state ($J = 9/2$) to a given state J' is given by

$$S_{ED}(J \rightarrow J') = \frac{3ch(2J+1)}{8\pi^3 \rho \bar{\lambda} e^2} \frac{\Gamma_\pi + 2\Gamma_\sigma}{\chi_\pi + 2\chi_\sigma} \tag{1}$$

where $\rho = 1.2 \times 10^{20}$ ions cm^{-3} is the Nd^{3+} concentration in the host crystal, $\bar{\lambda}$ is the mean wavelength of the transition and $2J + 1 = 10$ is the multiplicity of the ground state. $\Gamma_{\sigma,\pi}$ are the integrated absorbances and $\chi_{\sigma,\pi} = (n_{\sigma,\pi}^2 + 2)^2/(9n_{\sigma,\pi})$ the Lorentz local-field correction for the refractivity of the medium, where $n_\sigma = n_o$ (ordinary index) and $n_\pi = n_e$ (extraordinary index) have been obtained from reference [17]:

$$\begin{aligned} n_a(\lambda) \approx n_b(\lambda) \equiv n_o(\lambda) &= \sqrt{1 + \frac{2.2465\,\lambda^2}{\lambda^2 - 0.022\,6803}} \\ n_c(\lambda) \equiv n_e(\lambda) &= \sqrt{1 + \frac{2.41957\,\lambda^2}{\lambda^2 - 0.024\,5458}}. \end{aligned} \tag{2}$$

According to the JO theory, the line strength of any ED transition between two states J and J' can be written as

$$S_{ED}(J \rightarrow J') = \sum \Omega_t |\langle J||U^t||J'\rangle| \tag{3}$$

where Ω_t ($t = 2, 4, 6$) are the so-called JO intensity parameters (that characterize the strength of the crystal field) and the matrix elements $|\langle J||U^t||J'\rangle|$ (U^t being a tensor operator of rank t)

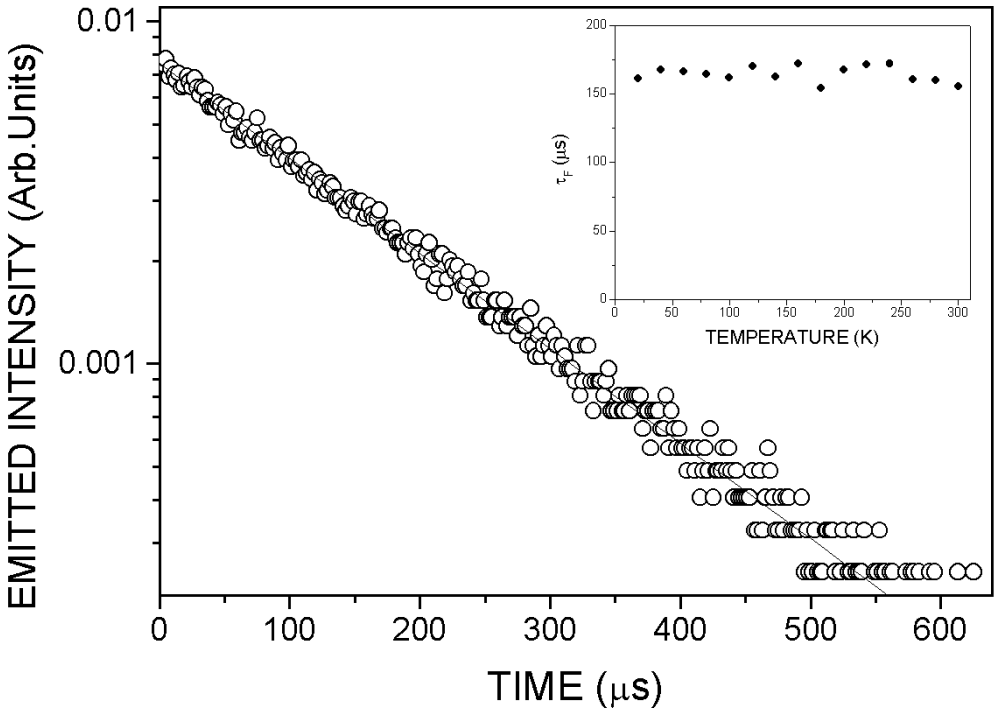

Figure 3. Time evolution of the room temperature $^4F_{3/2}$ fluorescence. The inset shows the fluorescence lifetime as a function of temperature.

are related to the free ion and can be obtained from the tables of Carnal and Rajnak [18]. Thus the JO intensity parameters can be obtained by fitting the latter expression to the values of S experimentally determined from expression (1).

Using the absorption spectra of figure 4, the JO intensity parameters $\Omega_2 = 6.15 \times 10^{-20}$ cm^2, $\Omega_4 = 6.79 \times 10^{-20}$ cm^2 and $\Omega_6 = 6.21 \times 10^{-20}$ cm^2 were obtained by a least-squares fitting. The estimated error between the experimental and calculated line strengths is about 5%.

Once the $\Omega_{2,4,6}$ JO parameters have been determined, the ED radiative emission probabilities $A(J \rightarrow J')$ for any pair of states can be calculated from

$$A(J \rightarrow J') = \frac{64\pi^4 e^2}{3h(2J+1)\overline{\lambda}^3}\left(\frac{2}{3}n_\sigma^2\chi_\sigma + \frac{1}{3}n_\pi^2\chi_\pi\right)S_{ED}(J \rightarrow J') \tag{4}$$

and, from this, the radiative lifetime defined as $\tau_R = (\sum A(J \rightarrow J'))^{-1}$ and the branching ratios $\beta_{J\rightarrow J'} = A(J \rightarrow J')\tau_R(J)$, of great relevance in laser efficiency, can be estimated. In addition, the quantum efficiency, $\eta = \tau_F/\tau_R$, of any state can be calculated by measuring its fluorescence lifetime (τ_F). Table 2 shows the ED radiative transition probabilities, branching ratios, quantum efficiency (using the fluorescence lifetime obtained from figure 3) and radiative lifetime for the metastable state $^4F_{3/2}$ of Nd^{3+} in $Gd_2(MoO_4)_3$. The values reported for other non-linear SFD laser crystals have been included in this table for comparison [19, 20]. Thus, under the JO formalism approach, Nd:$Gd_2(MoO_4)_3$ presents the highest quantum efficiency ($\simeq$0.95) among the SFD crystals. High quantum efficiency ensures a minimal thermal loading, since the non-radiative decays can be considered negligible [21]. This is an advantage over crystals with relatively low quantum efficiency (such as the well known Nd:$YAl_3(BO_3)_4$)

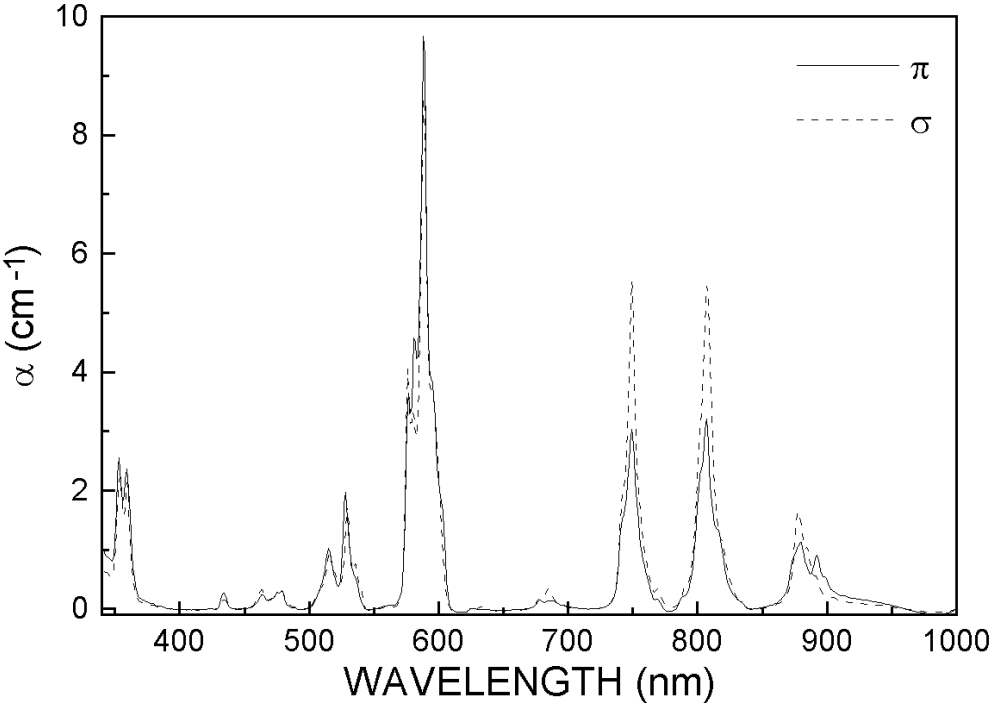

Figure 4. Room temperature polarized absorption spectra.

in which a substantial heating occurs during diode pumping for infrared and visible laser oscillation [21]. We can therefore conclude that the high quantum efficiency determined for the Nd:$Gd_2(MoO_4)_3$ system ensures that it can be incorporated in compact laser devices since heat dissipation is not necessary (at least for the crystal).

3.1.3. Room temperature emission spectra: determination of the spectroscopic quality parameter and stimulated emission cross section. Figure 5(a) shows the polarized emission spectra in the 850–1500 nm spectral range. The Nd:$Gd_2(MoO_4)_3$ crystal was excited by a Ti:sapphire laser tuned to 807 nm (where the absorption spectrum peaks). Only radiative emissions departing from the metastable $^4F_{3/2}$ state are detected. The final state corresponding to each band is indicated in the figure. The $^4F_{3/2} \rightarrow {}^4I_{15/2}$ transition is not shown due to its low emission intensity, as well as to experimental limitations. From this figure the branching ratios can be experimentally obtained by integrating the corresponding emission band and then dividing by the total integrated area. The β-values obtained by this way are 0.43, 0.45 and 0.11 for the transitions from the $^4F_{3/2}$ state to the $^4I_{9/2}$, $^4I_{11/2}$ and $^4I_{13/2}$ states respectively. By comparison with table 2, it should be noted that there is a reasonable agreement between the branching ratio values obtained from the Judd–Ofelt approximation and those obtained experimentally.

Analysis carried out in reference [3] has shown that the probability of spontaneous transitions $A_{JJ'}$ for the various $^4F_{3/2} \rightarrow {}^4I_{J'}$ transitions depends primarily on the intensity parameters Ω_t of the fourth and sixth orders, because the matrix element $\langle||U^{(2)}||\rangle$ for transitions between these states is equal to zero. Hence the intermanifold luminescence branching ratios $\beta_{JJ'}$ can be represented as dependent only on one parameter (the spectroscopic

Table 2. Spectral parameters (radiative rates, A, branching ratios, β, and radiative lifetimes, τ_R) for the $^4F_{3/2} \rightarrow {}^4I_J$ transitions of Nd^{3+} in different non-linear crystals, determined from the JO formalism. Experimental fluorescence lifetimes and calculated quantum efficiencies are also included.

Material	Transition	$A(J \rightarrow J')$ (s^{-1})	β	τ_R (μs)	τ_F (μs)	η
$MgO:LiNbO_3$	$^4F_{3/2} \rightarrow {}^4I_{9/2}$	4649	0.47	101.1	95	0.94
	$\rightarrow {}^4I_{11/2}$	4451	0.45			
	$\rightarrow {}^4I_{13/2}$	791	0.08			
	$\rightarrow {}^4I_{15/2}$		—			
$YAl_3(BO_3)_4$	$^4F_{3/2} \rightarrow {}^4I_{9/2}$	1637	0.493	302.1	52	0.18
	$\rightarrow {}^4I_{11/2}$	1430	0.431			
	$\rightarrow {}^4I_{13/2}$	235	0.071			
	$\rightarrow {}^4I_{15/2}$	12	0.005			
$LaBeGeO_5$	$^4F_{3/2} \rightarrow {}^4I_{9/2}$	1242	0.390	314.2	280	0.89
	$\rightarrow {}^4I_{11/2}$	1604	0.505			
	$\rightarrow {}^4I_{13/2}$	320	0.100			
	$\rightarrow {}^4I_{15/2}$	16	0.005			
$Gd_2(MoO_4)_3$	$^4F_{3/2} \rightarrow {}^4I_{9/2}$	2593	0.451	173	165	0.95
	$\rightarrow {}^4I_{11/2}$	2621	0.460			
	$\rightarrow {}^4I_{13/2}$	470	0.086			
	$\rightarrow {}^4I_{15/2}$	25	0.003			

quality parameter) which is defined as [3]

$$\chi({}^4F_{3/2}) = \frac{\Omega_4}{\Omega_6}. \tag{5}$$

Figure 5(b) shows the analytical dependence of the branching ratio as a function of the χ-value. Once the branching ratios have been experimentally determined, the spectroscopic quality parameter can be estimated. By inspection of figure 5(b) and using the β obtained experimentally (the dotted line in figure 5(b)), we found $\chi \approx 1.1$, this being in good agreement with Judd–Ofelt calculations: $\chi = \Omega_4/\Omega_6 = 1.09$.

Let us focus our attention onto the main laser channel $^4F_{3/2} \rightarrow {}^4I_{11/2}$. Once the branching ratios and radiative lifetime are known (see table 2) the spectral dependence of the stimulated emission cross section can be determined from the polarized fluorescence spectra according to the expression [22, 23]

$$\sigma_e^p(\lambda) = 3\lambda^5 \beta_J I^p(\lambda) \Big/ \left[8\pi n_p^2 c \tau_R \int \lambda \big(2I^\sigma(\lambda) + I^\pi(\lambda)\big)\, \mathrm{d}\lambda \right] \tag{6}$$

where λ is the emission wavelength, $I_p(\lambda)$ ($p = \sigma$ or π) the emission intensity for each wavelength, c the speed of light and n_p ($p = \sigma$ or π) the material refractive indices.

The spectral dependence of the stimulated emission cross section obtained from the emission spectra for the $^4F_{3/2} \rightarrow {}^4I_{11/2}$ laser channel is shown in figure 6. The calculated peak cross sections are $\sigma_\pi = 0.35 \times 10^{-19}$ cm^2 (at 1068.9 nm) and $\sigma_\sigma = 1.1 \times 10^{-19}$ cm^2 (at 1059.7 nm). These values are slightly lower than but of the order of those previously reported for other non-linear crystals (see table 2). As the threshold power for laser oscillation is proportional to $1/\sigma_e$ [24], the expected laser threshold should be higher than those of the other crystals reported in table 2.

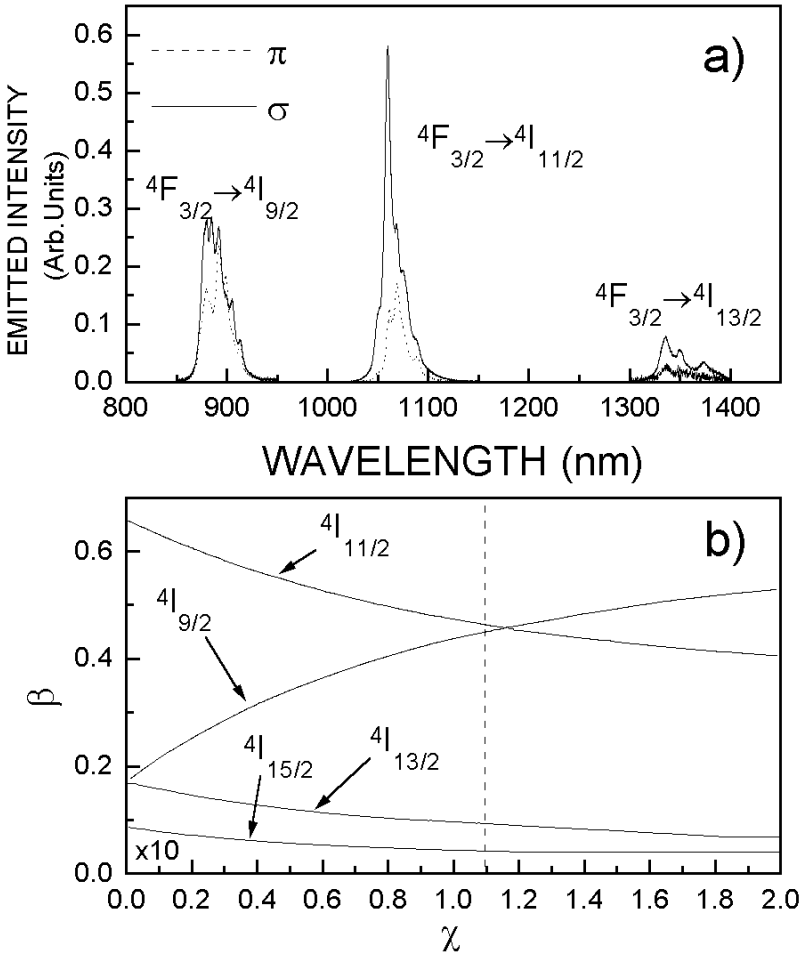

Figure 5. (a) The dependence of the radiative branching ratios of the $^4F_{3/2}$ state as functions of the spectroscopic quality parameter as defined in the text. (b) Polarized emission spectra obtained at room temperature after 800 nm excitation.

The spectral dependence of the emission cross section has also been determined for the $^4F_{3/2} \rightarrow {}^4I_{9/2}$ and $^4F_{3/2} \rightarrow {}^4I_{13/2}$ channels. The peak cross sections obtained are listed in table 3.

From figure 6, it can be predicted that only ordinary radiation will be obtained if a $Nd:Gd_2(MoO_4)_3$ crystal oriented perpendicular to its optical axis is placed in a laser cavity, since the highest gain is associated with σ-polarized emission. However, since the phase-matching direction is about 60° with respect to the optical axis, both σ and π polarizations contribute to the extraordinary radiation. In fact, the extraordinary effective cross section can be written as

$$\sigma_e = \sigma_\sigma \cos^2(60^\circ) + \sigma_\pi \cos^2(30^\circ). \tag{7}$$

As for the ordinary radiation (***E*** perpendicular to the c-axis), the effective cross section is simply $\sigma_o = \sigma_\sigma$.

Figure 7 shows the spectral dependence of the ordinary and extraordinary emission cross section obtained from expression (7) using σ_π and σ_σ data from figure 6. The polarized emission

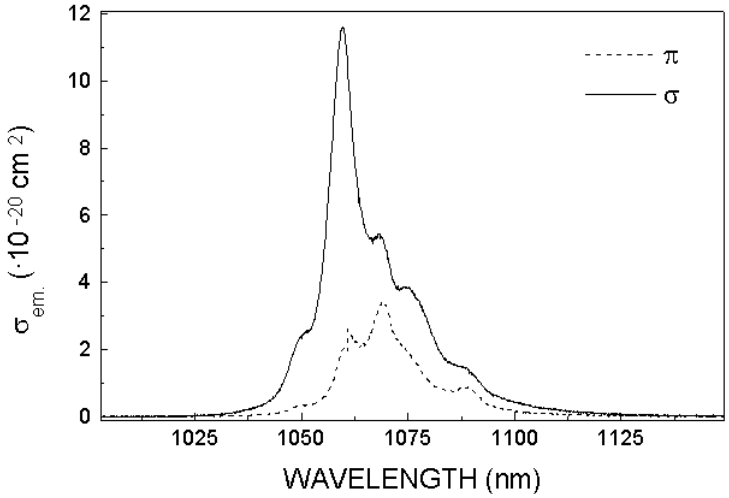

Figure 6. The spectral dependence of the polarized (σ and π) emission cross sections for the $^4F_{3/2} \rightarrow {}^4I_{11/2}$ laser channel.

Table 3. Polarized emission cross section peak values and spectral positions for the $^4F_{3/2} \rightarrow {}^4I_J$ transitions.

Transition	Polarization	σ (10^{-20} cm^2)	λ (nm)
$^4F_{3/2} \rightarrow {}^4I_{9/2}$	σ	0.56	884.3
	π	0.47	892.7
$^4F_{3/2} \rightarrow {}^4I_{11/2}$	σ	1.1	1059.7
	π	0.35	1068.9
$^4F_{3/2} \rightarrow {}^4I_{13/2}$	σ	0.15	1336.4
	π	0.05	1336.6

cross section along the phase-matching direction peaks at 1059.7 nm ($\sigma_o = 1.1 \times 10^{-19}$ cm^2) for ordinary polarization and at 1060.6 nm ($\sigma_e = 0.5 \times 10^{-19}$ cm^2) for extraordinary polarization.

It should be noted that the emission cross section reaches the maximum value for ordinary polarization. As was stated in section 2, $Gd_2(MoO_4)_3$ has a positive birefringence, so for the type I SHG process only extraordinary radiation contributes efficiently ($n_o(\lambda/2) = n_e(\lambda, 60^\circ)$). Thus, in order to produce visible radiation by means of SFD, extraordinary radiation is needed. However, only ordinary radiation, in principle, will be oscillating in the laser cavity because of its higher gain. It is therefore necessary to avoid this ordinary oscillation to ensure that the propagating radiation in the laser cavity will be extraordinarily polarized. This can be achieved by suitably placing a Brewster plate [12] or choosing appropriate geometrical conditions as for the case of $LiNbO_3$ [25].

Finally the polarized emission cross sections corresponding to the $^4F_{3/2} \rightarrow {}^4I_{11/2}$ laser channel obtained for different Nd-doped non-linear crystals are listed in table 4 [20]. The σ-polarized emission cross section obtained for the Nd:$Gd_2(MoO_4)_3$ system is comparable to those obtained for other laser crystals. On the other hand, the value obtained for the π-polarized emission cross section is $\sim$3 times lower in comparison to the other non-linear

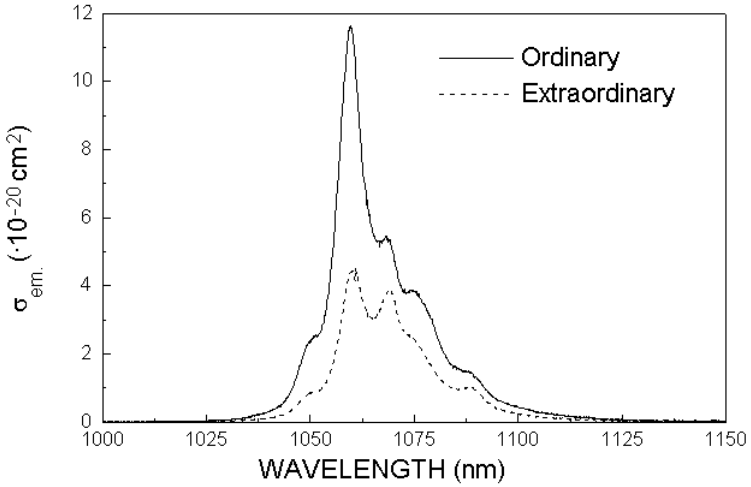

Figure 7. Ordinary and extraordinary emission cross sections corresponding to the $^4F_{3/2} \rightarrow {}^4I_{11/2}$ transition for a phase-matching orientated crystal.

Table 4. Polarized cross sections at emission peaks for Nd^{3+} ions in different non-linear crystals.

Material	Polarization	σ (10^{-19} cm^2)	λ (nm)
$MgO:LiNbO_3$	σ	0.78	1094
	π	2.7	1085
$YAl_3(BO_3)_4$	σ	0.97	1062
	π	1.37	1060
$LaBeGeO_5$	σ	0.76	1049
	π	1.13	1049
$Gd_2(MoO_4)_3$	σ	1.1	1060
	π	0.35	1069

crystals. This lower emission cross section indicates that the pump powers at threshold in $Nd:Gd_2(MoO_4)_3$ laser crystals are expected to be higher than for the other non-linear laser crystals. Nevertheless, infrared (IR) laser oscillation has been obtained in this laser system with relatively low thresholds [10, 12]. In addition, the peak emission wavelength could be interesting in relation to neodymium glass amplifiers.

3.1.4. Up-conversion luminescence. Excited-state absorption (ESA) of pump or laser radiation can lead to considerable losses in the laser gain [26]. Further, it can result in multiphonon relaxation processes, increasing the temperature of the laser crystal. ESA of laser radiation can be measured by so-called 'two-beam spectroscopy' [27] which is beyond the scope of this work. Information on the relevance of ESA of pump radiation can be partially obtained by investigating the IR-to-visible up-converted luminescence, which is typically observed in Nd-doped crystals [26, 28]. We have performed a systematic investigation of the IR-to-visible up-converted luminescence in the spectral region of interest for diode pumping (720 to 830 nm).

Figure 8 shows the unpolarized RT visible emission spectrum obtained under 808 nm excitation (a peak wavelength in the absorption spectrum). As can be observed, the emission spectrum consists of three structured bands tentatively assigned to the spin-allowed transitions from the states $^4G_{7/2}$ and $^4G_{11/2}$ to the terminal states $^4I_{9/2}$ (the band centred at 530 nm), $^4I_{11/2}$ (the band centred at 600 nm) and $^4I_{13/2}$ (the band centred at 530 nm).

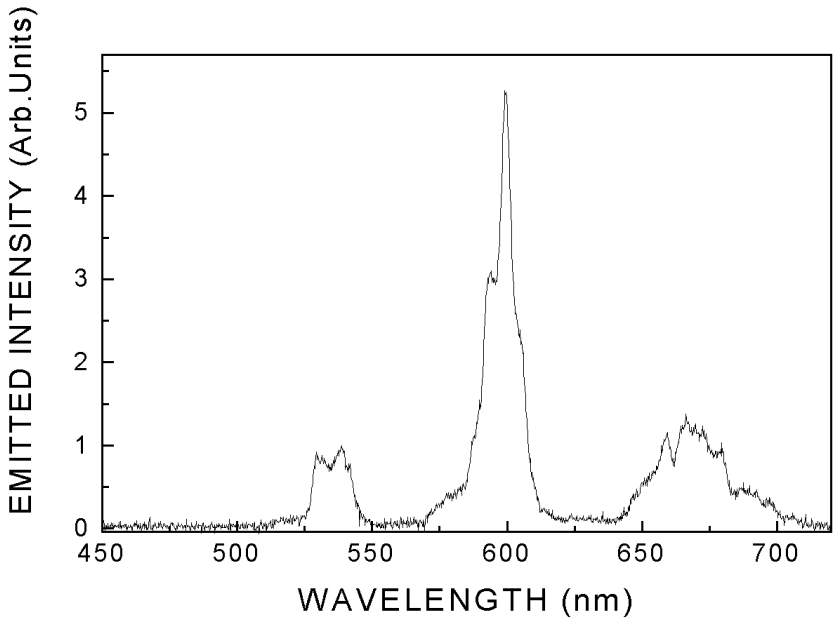

Figure 8. The unpolarized emission spectrum in the visible region after pumping at 808 nm.

In order to populate the $^4G_{7/2}$ and $^4G_{11/2}$ excited states, non-linear processes involving two pump photons are necessary. In principle, two different mechanisms could be responsible for the population of these states: a sequential ESA of two pump photons by each Nd^{3+} ion or an energy-transfer up-conversion (ETU) process.

In the case of an ETU process, the intensity of the visible luminescence is proportional to the square of the population of the metastable state $^4F_{3/2}$. As a consequence, in this case the up-converted luminescence excitation intensity is proportional to the square of the absorbance. On the other hand, ESA of pump photons requires resonant absorption from the metastable state of each Nd^{3+} ion. In this second case the excitation spectrum of the visible luminescence consists of a modulation of the (first-photon) absorption spectrum by the second-photon absorption spectrum [29].

Figure 9 shows the up-converted luminescence excitation spectrum together with the spectrum of the square of the absorbance. As can be observed, these two spectra display quite similar shapes. Nevertheless, there are several resonant absorptions which have been marked by arrows (742, 744, 747, 802 and 805 nm). For these wavelengths the up-conversion luminescence is produced on the basis of an ESA process. This is in contrast to the case for other non-linear laser crystals such as $Nd:YAl_3(BO_3)_4$, for which ETU was found to be the only mechanism responsible for the up-conversion luminescence [28].

From figure 9 we can conclude that in $Nd:Gd_2(MoO_4)_3$ for most of the pump wavelengths the ETU process is dominant, although for some pump wavelengths the up-conversion luminescence originates from both ETU and ESA processes. The location of these pump

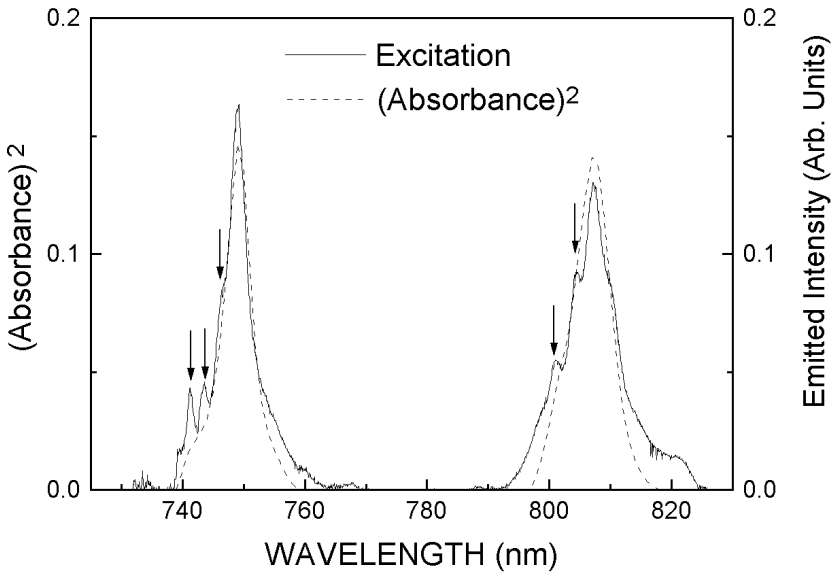

Figure 9. The 600 nm excitation spectrum in the 750–850 nm spectral range. The spectrum of the square of the absorbance is also displayed. The resonant wavelengths producing ESA of pump radiation are indicated by arrows.

wavelengths is of special importance in laser gain experiments. It has been previously reported that if pumping is achieved at a wavelength for which ESA is produced, a drastic reduction in the laser slope efficiency occurs [26]. Thus our study of the up-conversion luminescence in this crystal is of particular relevance for determining optimum pump wavelengths.

3.2. Laser gain experiments

In this section, we will discuss laser gain experiments that have been carried out in order to determine the conditions needed for efficient infrared and visible laser light generation. The experimental details of the laser cavity have already been described in section 2. For laser gain experiments a Nd:$Gd_2(MoO_4)_3$ crystal orientated along the phase-matching direction was used.

The spectral distribution of the IR output laser radiation is shown in figure 10 for two different output coupling transmittances. The pump power was 500 mW, which is similar to typical output power values available in low-current diodes. The cavity length was set to 9 cm, providing the lowest pump power at the oscillation threshold [24]. The dotted line corresponds to the output beam obtained by using a 0.36% output coupler. For this transmittance the intracavity infrared power is maximum. This, in principle, should lead to a high infrared-to-visible efficiency. However, no visible radiation was observed under these conditions. In fact, for this output coupler transmittance, several lines were oscillating in the cavity. This multiline oscillation produces high output power instabilities. In addition, the output laser beam was 100% ordinarily polarized (independently of the laser cavity geometry). As a consequence, no green laser light was observed, since for SHG, extraordinary laser radiation is needed. The multiline laser oscillation can be explained on the basis of the relatively broad emission spectrum shown in figure 7 in such a way that the gain associated with several spectral modes is above threshold.

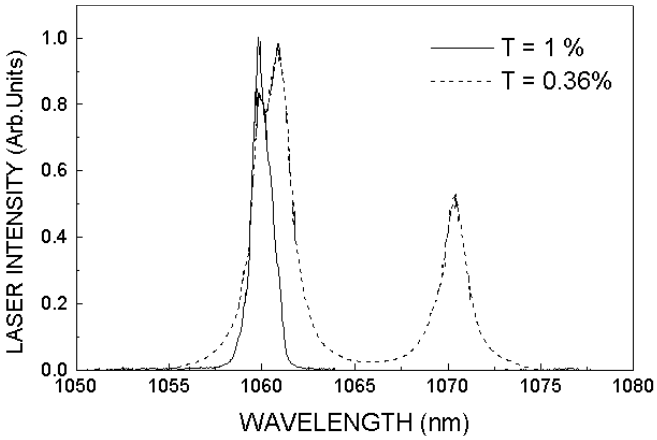

Figure 10. The spectral distribution of the output laser radiation as a function of the output mirror transmittance (0.36%: dotted line; 1%: solid line).

This multiline laser oscillation can therefore be avoided by increasing the laser threshold. The solid line in figure 10 shows the spectral distribution of the output laser beam when the output coupler transmittance is 1% and the cavity is aligned such that output power is at maximum. On changing the output coupler transmittance from 0.36 to 1%, the pump threshold is increased and only the highest gain line is oscillating. Under these conditions, the laser radiation was ordinarily polarized and the laser wavelength was 1059.7 nm. This is in accordance with the emission cross section spectrum shown in figure 6, which peaks for ordinary polarization at this wavelength. When the 1% output coupler is used, the laser power becomes stable, since the competition between different laser lines has been avoided. The spectral shape of the laser radiation has also been measured for transmittances higher than 1%; it shows no changes from that obtained for the 1% coupler (the solid line in figure 10). Therefore when $Nd:Gd_2(MoO_4)_3$ is to be integrated in a laser device, special care must be taken when choosing the output coupler; if stability and monochromatic laser radiation are desired, the output coupler transmittance should be higher than 1%.

Finally, green laser radiation was obtained by SFD only when the 1% output coupler was used. The desired (extraordinary) polarization of the laser radiation was achieved by changing the geometrical conditions in our experimental laser cavity. The cavity length was reduced from 9 to 5 cm and the output coupler was slightly aligned according to the method previously reported for $LiNbO_3$ [25]. A 100% extraordinary infrared radiation was then obtained at a laser wavelength of 1060.6 nm in accordance with results displayed in figure 7. The observed green radiation power was of the order of some μW. Laser polarization control based on adjustments of the cavity geometry and crystal birefringence is a well known method, which was first reported in relation to $LiNbO_3$ [25].

4. Conclusions

In this work, basic spectroscopy at low and room temperature has been used to determine physical parameters of relevance in laser dynamics of the Nd^{3+}:β'-$Gd_2(MoO_4)_3$ non-linear system. Low-temperature experiments provided a complete table of the energy levels of Nd^{3+} ions. The presence of two non-equivalent Nd centres in the crystal lattice has also been deduced from the low-temperature experiments. On the other hand, room temperature

absorption and emission experiments have been performed in order to estimate the main properties of metastable states of relevance in laser dynamics. The Judd–Ofelt formalism has been used to calculate the emission branching ratios, emission cross sections and quantum efficiency. The emission cross sections have been found to be of the same order as for other non-linear laser crystals on the basis of Nd doping. The high quantum efficiency determined in this work ($\simeq 1$) makes Nd^{3+}:β'-$Gd_2(MoO_4)_3$ a promising material for application in high-power integrated lasers in the visible, since no thermal loading is expected. IR-to-visible up-conversion luminescence has been reported, and the mechanism responsible discussed. From this discussion, the optimum pump wavelengths for diode pumping have been determined—avoiding in this way undesirable reductions in the laser slope efficiency. Finally, laser gain experiments have been performed and the optimum conditions for visible laser light and stable IR generation determined.

Acknowledgments

This work was sponsored by the Comisión Interministerial de Ciencia y Tecnología (CICyT) under project No PB97-0033 and by the 'Integrated Action' project of Germany and Spain.

References

[1] Lin J T 1990 *Laser Optron.* **9** 34–40
[2] Lin J T and Kato K 1990 *Proc. SPIE, vol 1270* 58–63
[3] Kaminskii A A 1996 *Crystalline Lasers* (New York: CRS Press)
[4] Borchardt H J and Bierstedt P E 1966 *Appl. Phys. Lett.* **8** 50
[5] Aizu K, Kumada A, Yumoto H and Asida S 1969 *J. Phys. Soc. Japan* **27** 511
[6] Smith A W and Barns G 1969 *Phys. Lett.* A **28** 501
[7] Cummins S E 1970 *Ferroelectrics* **1** 11
[8] Kaminskii A A 1995 *Phys. Status Solidi* a **149** K39
[9] Nishioka H, Odajima W, Tateno M, Ueda K, Kaminskii A A, Butashin A V, Bagaev S N and Pavlyuk A 1997 *Appl. Phys. Lett.* **70** 1366–8
[10] Kaminskii A A, Bagaev S N, Ueda K, Pavlyuk A A and Musha M 1997 *Quantum Electron.* **27** 675–6
[11] Kaminskii A A, Eichler H-J, Grebe D, Macdonald R, Bagaev S N, Pavlyuk A A and Kuznetsov F A 1996 *Phys. Status Solidi* a **153** 1
[12] Kaminskii A A, Butashin A V, Eichler H-J, Grebe D, Macdonald R, Ueda K, Nishioka H, Odajima W, Tateno M, Song J, Musha M, Bagaev S N and Pavlyuk A A 1997 *Opt. Mater.* **7** 59–73
[13] Kaminskii A A 1981 *Laser Crystals* (Berlin: Springer)
[14] Henderson B and Imbusch G F 1989 *Optical Spectroscopy of Inorganic Solids (Oxford Science Publications)* (Oxford: Clarendon)
[15] Judd B R 1962 *Phys. Rev.* **127** 750
[16] Ofelt G S 1962 *J. Chem. Phys.* **37** 511
[17] Singh S, Potopowicz J R, Bonner W A and Van Uitert L G 1971 *Handbook of Lasers* (Cleveland, OH: Chemical Rubber Company Press)
[18] Carnal W T and Rajnak K 1968 *J. Chem. Phys.* **49** 4422
[19] Jaque D, Capmany J, Luo Z D and García Solé J 1997 *J. Phys.: Condens. Matter* **9** 9715
[20] Jaque D, Capmany J, Sanz García J A, Brenier A, Boulon G and García Solé J 1999 *Opt. Mater.* **13** 147–57
[21] Jaque D, Capmany J, Rams J and García Solé J 1999 *J. Appl. Phys.* **87** 1042–8
[22] Singh S, Smith R G and Van Uitert L G 1974 *Phys. Rev.* B **10** 2566
[23] Aull B F and Jenssen H P 1982 *IEEE J. Quantum Electron.* **18** 925
[24] Risk W P 1988 *J. Opt. Soc. Am.* B **5** 1412
[25] Capmany J, Jaque D and García Solé J 1999 *Opt. Commun.* **161** 253
[26] Chuan T and Verdún H 1996 *IEEE J. Quantum Electron.* **32** 79
[27] Jaque D, García Solé J, Brenier A, Boulon G and Luo Z D 2000 *Eur. Phys. J. Appl. Phys.* **10** 29
[28] Jaque D, Capmany J, Molero F, Luo Z D and García Solé J 1998 *Opt. Mater.* **10** 211
[29] Kliewer M L and Powell R C 1989 *IEEE J. Quantum Electron.* **25** 8